

Subtle Differences in Virus Composition Affect Disinfection Kinetics and Mechanisms

Thérèse Sigstam, Greg Gannon, Michele Cascella, Brian M. Pecson, Krista Rule Wigginton and Tamar Kohn
Appl. Environ. Microbiol. 2013, 79(11):3455. DOI:
10.1128/AEM.00663-13.
Published Ahead of Print 29 March 2013.

Updated information and services can be found at:
<http://aem.asm.org/content/79/11/3455>

SUPPLEMENTAL MATERIAL	<i>These include:</i>
	Supplemental material
REFERENCES	This article cites 40 articles, 9 of which can be accessed free at: http://aem.asm.org/content/79/11/3455#ref-list-1
CONTENT ALERTS	Receive: RSS Feeds, eTOCs, free email alerts (when new articles cite this article), more»

Information about commercial reprint orders: <http://journals.asm.org/site/misc/reprints.xhtml>
To subscribe to to another ASM Journal go to: <http://journals.asm.org/site/subscriptions/>

Subtle Differences in Virus Composition Affect Disinfection Kinetics and Mechanisms

Thérèse Sigstam,^a Greg Gannon,^b Michele Cascella,^b Brian M. Pecson,^a Krista Rule Wigginton,^{a*} Tamar Kohn^a

Laboratory of Environmental Chemistry, School of Architecture, Civil and Environmental Engineering (ENAC), École Polytechnique Fédérale de Lausanne (EPFL), Lausanne, Switzerland^a; Laboratory of Computational Chemistry and Biochemistry, Department of Chemistry and Biochemistry, University of Bern, Bern, Switzerland^b

Viral disinfection kinetics have been studied in depth, but the molecular-level inactivation mechanisms are not understood. Consequently, it is difficult to predict the disinfection behavior of nonculturable viruses, even when related, culturable viruses are available. The objective of this work was to determine how small differences in the composition of the viral genome and proteins impact disinfection. To this end, we investigated the inactivation of three related bacteriophages (MS2, fr, and GA) by UV₂₅₄, singlet oxygen (¹O₂), free chlorine (FC), and chlorine dioxide (ClO₂). Genome damage was quantified by PCR, and protein damage was assessed by quantitative matrix-assisted laser desorption ionization (MALDI) mass spectrometry. ClO₂ caused great variability in the inactivation kinetics between viruses and was the only treatment that did not induce genome damage. The inactivation kinetics were similar for all viruses when treated with disinfectants possessing a genome-damaging component (FC, ¹O₂, and UV₂₅₄). On the protein level, UV₂₅₄ subtly damaged MS2 and fr capsid proteins, whereas GA's capsid remained intact. ¹O₂ oxidized a methionine residue in MS2 but did not affect the other two viruses. In contrast, FC and ClO₂ rapidly degraded the capsid proteins of all three viruses. Protein composition alone could not explain the observed degradation trends; instead, molecular dynamics simulations indicated that degradation is dictated by the solvent-accessible surface area of individual amino acids. Finally, despite the similarities of the three viruses investigated, their mode of inactivation by a single disinfectant varied. This explains why closely related viruses can exhibit drastically different inactivation kinetics.

Many important illnesses such as gastroenteritis, poliomyelitis, aseptic meningitis, and some variants of hepatitis can be transmitted by viruses via the fecal-oral route (1). Contact with pathogenic viruses can occur when humans are exposed to drinking or recreational water that has been impacted by wastewater. To prevent viral disease outbreaks, it is therefore important that water be appropriately treated before it is brought into contact with humans.

Inactivation kinetics of viruses upon treatment by various disinfectants, including UV, singlet oxygen (¹O₂), free chlorine (FC), chloramines, and chlorine dioxide (ClO₂) have been studied in depth (2–8). Even though these disinfectants have been used for decades or even centuries, we still lack a fundamental understanding of their mode of action. Several studies have investigated the role of damage to either the viral genomes or proteins, but rarely were the two considered simultaneously. Consequently, different studies reach different conclusions regarding the important disinfection targets. For example, it has been postulated elsewhere (9, 10) that chlorine dioxide and free chlorine inactivate poliovirus and hepatitis A virus, respectively, by damaging the viral genome. Contradictorily, Lim et al. (2) report that genome damage is not sufficient to explain inactivation by chlorine dioxide. This is supported by the work of Napolitano et al., who suggested that inactivation should be due to protein damage, as ClO₂ reacts more readily with amino acids than with nucleotides (11). UV is often reported to cause fatal genome damage by forming pyrimidine dimers (4, 12, 13), and yet protein damage has also been reported (14, 15). Singlet oxygen has been found to cause protein cross-linking (16), whereas other studies report genome damage as the main target for disinfection (17, 18).

Interestingly, different serotypes within a family of viruses can exhibit very different susceptibilities to disinfectants. For example, the inactivation of coxsackievirus A9 by free chlorine was 10 to

44 times more rapid than the inactivation of coxsackievirus B5, depending on the pH (3). Similarly, UV₂₅₄ inactivation of adenovirus type 41 was significantly slower than that for adenovirus types 2 and 5 (19). These substantial differences in inactivation kinetics arise even though the serotypes exhibit only minor differences in composition. To explain this behavior, the molecular-level effects of the disinfectants on the different virus components must be understood.

The present work's goal was to assess how subtle changes in the composition of three closely related viruses affect the kinetics of inactivation by these disinfectants and to determine to what extent the observed differences can be explained by damage incurred by the viral genomes and capsid proteins. Specifically, we compared the inactivation of MS2 with that of two other phages of the *Leviviridae* family, fr and GA. These phages serve as ideal models for this work as they are among the most simply structured viruses: they consist of a positive-sense, single-stranded RNA genome (approximately 3,500 nucleotides), which is surrounded by an icosahedral capsid containing 180 copies of a capsid protein (composed of 129 amino acids), as well as one copy of an assembly protein (A protein; composed of 393 amino acids in MS2 and fr

Received 1 March 2013 Accepted 24 March 2013

Published ahead of print 29 March 2013

Address correspondence to Tamar Kohn, tamar.kohn@epfl.ch.

* Present address: Krista Rule Wigginton, University of Michigan, Department of Civil and Environmental Engineering, Ann Arbor, Michigan, USA.

Supplemental material for this article may be found at <http://dx.doi.org/10.1128/AEM.00663-13>.

Copyright © 2013, American Society for Microbiology. All Rights Reserved.

doi:10.1128/AEM.00663-13

and 390 amino acids in GA). The genomes of fr and GA are 85 and 74% identical to that of MS2, respectively, while the capsid proteins are 87 and 62% homologous, respectively (see Fig. S1 in the supplemental material) (20). Differences in the A protein composition are more pronounced, with MS2 and fr exhibiting 78% homology and MS2 and GA exhibiting 38% homology. The ultimate goal was to establish how these differences in capsid and genome content influence the kinetics and mechanisms of inactivation upon treatment by different disinfectants.

MATERIALS AND METHODS

Virus inactivation experiments were conducted using three different phages (MS2, fr, and GA) and four disinfectants (UV₂₅₄, ¹O₂, FC, and ClO₂). All experiments were conducted in stirred dilution buffer (DB; 5 mM PO₄²⁻, 10 mM NaCl, pH 7.4). At several time points during the inactivating treatment, samples were analyzed for the remaining virus infectivity, genome damage, and protein damage.

A complete list of all chemicals and reagents can be found in the supplemental material.

Microorganisms. Bacteriophage MS2 (DSMZ 13767) and its *Escherichia coli* host (DSMZ 5695) were purchased from the German Collection of Microorganisms and Cell Cultures (Braunschweig, Germany). Bacteriophage fr (ATCC 15767-B1) was purchased from LGC Standards (Molsheim, France). Bacteriophage GA was kindly provided by Joan Jofre (University of Barcelona). GA and fr were cultured in the same *E. coli* host as was MS2. They were propagated as described previously (17), and infectivity was assessed by enumeration of PFU using the double agar layer method (21). *E. coli* C-3000 (ATCC 15597) was purchased from LGC Standards (Molsheim, France) for the propagation of isotopically ¹⁵N-labeled bacteriophages (described in the supplemental material).

Disinfection experiments. All experiments pertaining to disinfection kinetics and genome damage were conducted in duplicate (two separate experiments for each combination of virus and disinfectant). The experiments were carried out in DB with a starting virus concentration of 1×10^{10} PFU/ml. Throughout the disinfection experiments, sample aliquots of 10 to 100 μ l were periodically removed and infective viruses were enumerated. A second set of aliquots (10 to 100 μ l) was collected for genome extraction and analysis as described below.

Protein damage assessment was performed in triplicate with sacrificial reactors (three sets of 3 to 4 reactors for each combination of virus and disinfectant). MS2 experiments were carried out in DB containing 5×10^{11} PFU/ml for UV₂₅₄ and ¹O₂ and 1×10^{11} PFU/ml for FC and ClO₂. Initial concentrations of fr and GA were 10-fold lower, due to the lower concentrations of the viral stock solutions. The disinfection process in each sacrificial reactor was halted at a given time point, and sample aliquots (10 to 100 μ l) were removed to enumerate infective viruses. The remainder of the sample was processed for protein quantification as described below.

UV₂₅₄. Black reactors (5 ml) containing 2-ml virus samples were placed in black plastic tubes (3 cm in diameter and 17.5 cm in height) to optimize beam collimation, as described previously (22). A low-pressure 18-W UV-C lamp (253.7 nm; model TUV T8; Philips) in a quasiparallel beam setup was used to inactivate the phages. Samples were exposed to UV₂₅₄ irradiance for periods between 0 and 10 min. The disinfection process was halted by removing the sample from the light source. The fluence entering the reactor was measured by actinometry (23) and corresponded to 2.4 W/m² for all experiments except for the protein damage assessment of MS2, which was performed at a fluence of 23 W/m².

Singlet oxygen. One hundred microliters of a 50-mg/liter Rose Bengal (RB) solution was added to 2-ml virus samples, and reactors were exposed for periods between 0 and 45 min to light emitted from a Sun 2000 solar simulator (ABET Technologies, Milford, CT) equipped with a 1-kW Xe lamp and an AM1.5 and a UVB cutoff filter (17). To compensate for RB photobleaching during the course of the experiments, 40 μ l and 27 μ l of the RB stock solution were added to the samples after 15 and 30 min,

respectively. This enabled maintenance of a stable singlet oxygen concentration of 1.1×10^{-11} M (3.52×10^{-7} mg/liter) as determined by reaction with the probe compound furfuryl alcohol (6). Disinfection was halted by removing the reactors from the light source. Control experiments conducted in the absence of light or RB did not show any inactivation.

Free chlorine. Ten-milliliter virus samples containing FC (1.5 to 3 mg/liter FC) were stirred in chlorine-demand-free beakers (prepared by overnight soaking in concentrated FC solution). The FC concentration was monitored with the *N,N*-diethyl-*p*-phenylenediamine (DPD) colorimetric method (21), and FC loss throughout the kinetic experiments did not exceed 15%. To halt the disinfection process, samples were diluted into a 9-fold volume of Tris buffer (10 mM Tris, pH 7.4) to quench the FC.

Chlorine dioxide. Chlorine dioxide was produced by mixing 100 ml 4% K₂S₂O₈ with 100 ml 2% NaClO₂ (24) and was stored at 4°C. The resulting ClO₂ stock concentration (250 to 1000 mg/liter) was determined by spectrophotometry ($\epsilon_{358 \text{ nm}} = 1,200 \text{ M}^{-1} \text{ cm}^{-1}$) (25). Prior to experiments, the stock solution was diluted to a working solution of 0.5 to 2 mg/liter ClO₂ and was spiked with virus stock solution to the desired virus concentration. To compensate for ClO₂ evaporation and consumption throughout the experiment, concentrated ClO₂ (16 mg/liter) was added at a rate of 20 μ l/min by means of a peristaltic pump (KdScientific). To halt the disinfection, ClO₂ was quenched by addition of sodium thiosulfate (0.63 M) at a 20:1 sample/quenching agent ratio. Control samples confirmed that the addition of sodium thiosulfate did not result in inactivation. However, thiosulfate was found to back-reduce oxidized protein residues; therefore, for the assessment of protein damage, disinfection experiments were conducted by the one-time addition of ClO₂, which was then left to evaporate. To achieve different ClO₂ doses, experiments were conducted in reactors with a range of initial ClO₂ concentrations (0.4 to 1.6 mg/liter).

Analysis of disinfection kinetics. For free chlorine, singlet oxygen, and UV₂₅₄, inactivation kinetics were fitted to a first-order Chick-Watson model (equation 1):

$$\ln \frac{C_v}{C_{v,0}} = -k_{CW} C_d t \quad (1)$$

where k_{CW} is the inactivation rate constant, C_d is the disinfectant concentration or UV₂₅₄ intensity (constant over the time of reaction), and C_v is the concentration of infective virus. For ClO₂, virus inactivation was described by the Hom model according to the following equation (equation 2):

$$\ln \frac{C_v}{C_{v,0}} = -k_H C_d^n t^{m-1} \quad (2)$$

where k_H is the Hom rate constant [$(\text{mg liter}^{-1} \text{ s}^{m-1})^{-1}$], n is the dilution coefficient (set to 1, as only a single ClO₂ concentration was used), and m is the constant for the inactivation rate law that describes the deviation from the ideal Chick-Watson model (equation 1). The parameters for the Hom model were fitted in Sigmaplot (version 12.0, 2011).

RNA extraction and qPCR. Two-hundred-microliter RNA samples were extracted with a PureLink viral RNA-DNA kit (Invitrogen). Extracts were reverse transcribed and amplified with a Rotorgene 3000 quantitative PCR (qPCR) platform (Corbett Life Science, Sydney, Australia) as described previously (17). For each virus, several genome segments (amplicons) were amplified, such that approximately 50% of the genome was covered. Details pertaining to the location and length of each amplicon analyzed, as well as the thermocycles used during the amplification, are given in Table S1 and Fig. S2 in the supplemental material. RNA standards were prepared for all viruses as described previously (17).

Quantification of genome integrity and degradation. The integrity of each amplicon was assessed, and the results were extrapolated as described by Pecson et al. (26) to quantify damage across the whole genome. Briefly, the probability of finding an intact amplicon i after a given level of inactivation corresponds to $n_i/n_{i,0}$ for each amplicon, where $n_{i,0}$ and n_i represent the number of intact genome copies detected before and after treat-

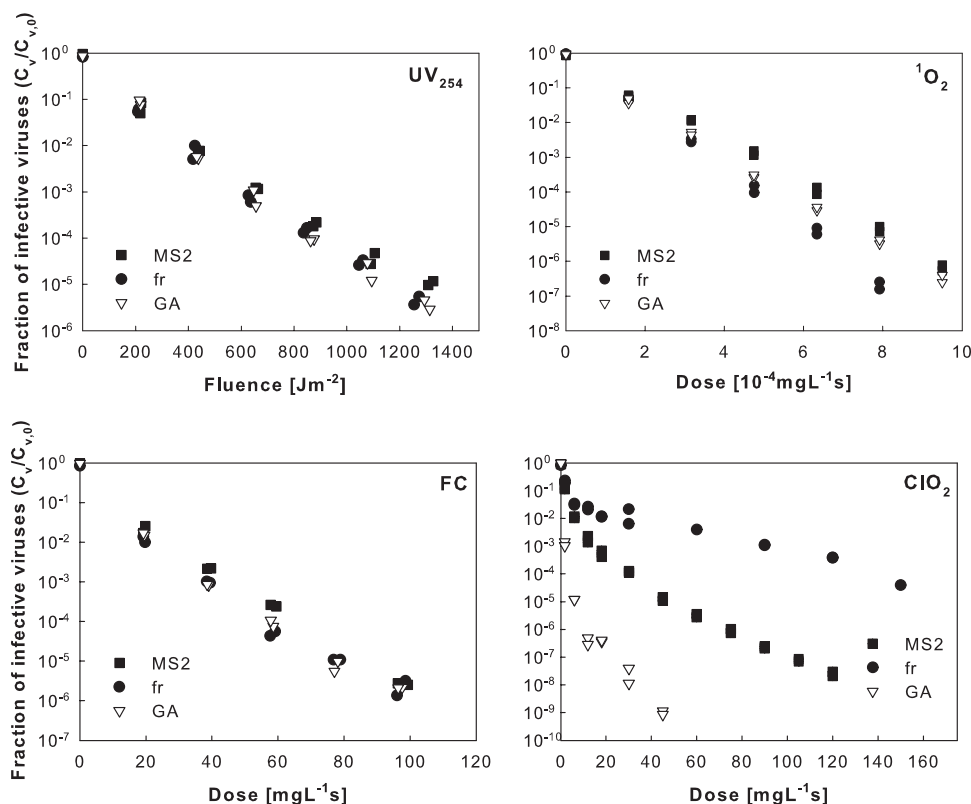


FIG 1 Comparison of disinfection kinetics of the three phages upon treatment by the four disinfectants investigated. Statistically significant differences in inactivation were found for the combinations indicated: UV_{254} , GA-MS2 ($P = 0.027$); 1O_2 , MS2-fr ($P < 0.001$), MS2-GA ($P = 0.022$), fr-GA ($P < 0.001$); ClO_2 , MS2-fr ($P = 0.026$), MS2-GA ($P = 0.007$), fr-GA ($P = 0.001$).

ment, respectively. The probability of all tested amplicons being intact in one genome copy then corresponds to $\prod n_i/n_{i,0}$. The probability that an entire RNA genome is intact, N/N_0 , can be extrapolated according to the following relationship (equation 3):

$$N/N_0 = \left(\prod n_i/n_{i,0} \right)^{\left(\frac{\text{genome length}}{\text{total length of } i \text{ amplicons}} \right)} \quad (3)$$

This extrapolation is valid only if the damage is evenly distributed across the entire genome or if a large fraction of the entire genome is assayed. In this study, we measured approximately half of the entire genome, a strategy that we have previously shown to account for variability in the distribution of damage across the genome (26).

Genome degradation rate constants (k_G) were determined from first-order fits of genome degradation versus disinfectant dose ($C_d t$) (equation 4) (27):

$$\ln \frac{N}{N_0} = -k_G C_d t \quad (4)$$

To determine if significant differences existed between genome degradation and inactivation of each phage, or if genome degradation or inactivation differed among the three phages, rate constants were compared by analysis of covariance (ANCOVA) analysis, whereby a P value of < 0.05 was deemed significant.

Analysis of peptide damage by MALDI. All matrix-assisted laser desorption ionization (MALDI) measurements were performed with an ABI 4800 MALDI tandem time of flight (TOF-TOF) mass spectrometer (Applied Biosystems, Rotkreuz, Switzerland), using the instrument settings and sample deposition methods described previously (14).

After disinfection, each sample was spiked with its corresponding untreated ^{15}N -labeled virus, where it served as an internal standard for quantification of the MALDI measurements. If necessary, the spiked samples

were first concentrated to 2 ml (for FC and ClO_2) with 100-kDa Microcon centrifugal filters (Millipore, Billerica, MA). Then, the samples were split into two parts, one for trypsin and one for chymotrypsin digestion. Prior to digestion, samples were concentrated to a final volume of 20 μ l. Of these, 2 μ l was removed and subjected to MALDI linear mode analysis to detect cleavage products of the capsid protein.

The concentrated samples were denatured for 10 min at 95°C. Cysteines were immediately acetylated with fresh iodoacetamide (5 μ l, 25 mM, in Tris buffer [50 mM, pH 8]) at 37°C in the dark for 60 min, to prevent oxidation. Excess iodoacetamide was then quenched with cysteine (5 μ l, 50 mM, in Tris buffer [50 mM, pH 8]), and the samples were incubated for 15 min in the dark. Finally, 25 μ l Tris buffer (50 mM, pH 8) containing 2 mM $CaCl_2$ was added to the samples, and they were digested overnight with freshly prepared trypsin or chymotrypsin at a 50:1 capsid protein-to-enzyme ratio. Prior to analysis, pure acetonitrile was added to the digested samples to enhance crystallization on the MALDI plate. Samples were then subjected to MALDI analysis in reflectron mode. The *in silico* digestion products for each proteolytic enzyme (PeptideMass software, Swiss-Prot database) are shown in Table S2 in the supplemental material. Table S3 shows the masses ($M + 1$) of each analyzed peptide and the mass of its corresponding ^{15}N -labeled peptide. For MS2, MALDI analysis covered 98% of the capsid protein, whereas fr and GA had coverages of 100 and 93%, respectively.

Calibration curves for each peptide were established using digested samples with known ^{14}N -/ ^{15}N -labeled virus ratios. The ratio of the ^{14}N / ^{15}N MALDI peak intensities was proportional to the ratio of native to heavy virus concentrations, as discussed elsewhere (28) (see Fig. S3 in the supplemental material). The peptide degradation during disinfection was then quantified by monitoring the change in ^{14}N / ^{15}N peak intensity ratio with increasing disinfectant doses.

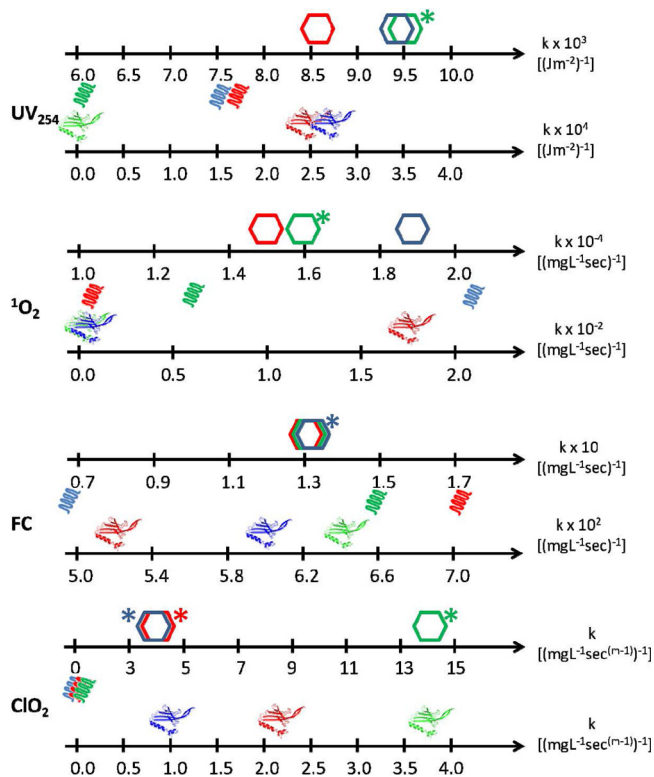


FIG 2 Overview of the inactivation rate constants (hexagons, upper scale), genome degradation rate constants (spirals, upper scale), and protein degradation rate constants (protein monomers, lower scale) for all four disinfecting treatments. Values for MS2 are shown in red, those for fr are shown in blue, and those for GA are shown in green. The asterisks indicate virus-treatment pairs where genome degradation could not account for inactivation. Exact values and associated errors are listed in Table 1 (inactivation) and Table 2 (genome and protein damage).

Degradation rate constants for individual peptides (k_{peptide}) were determined as a function of inactivation, according to equation 5:

$$\ln \frac{p}{p_0} = -k_{\text{peptide}} \log C_v / C_{v,0} \quad (5)$$

where p indicates a specific capsid protein peptide concentration at time t . Selected peptide products were subjected to tandem mass spectrometry (MS/MS) analysis in order to determine which amino acids within the peptide were modified during disinfection.

In addition to capsid proteins, the A protein of GA was analyzed following disinfecting treatments with UV_{254} and $^1\text{O}_2$. After reactions were quenched, the A proteins were separated from the more abundant capsid proteins with SDS-PAGE using 12% polyacrylamide gels and Coomassie blue staining (28, 29). The A protein lane (42 kDa) was cut and immediately subjected to cysteine acetylation followed by in-gel digestion with trypsin (30). The *in silico* digestion products of the GA A

protein (PeptideMass software, Swiss-Prot database) are shown in Table S4 in the supplemental material. Due to the low abundance of the A protein in GA compared to the capsid protein (one copy of A protein versus 180 copies of the capsid protein), only 15% of the A protein's 390 amino acids could be detected. Furthermore, ^{15}N -labeled internal standards could not be used for A protein analysis, because labeled A protein concentrations were too low for MALDI detection. Instead, peptide peak intensities were normalized to that of an A protein peptide presumed stable (due to the absence of residues susceptible to UV_{254} or $^1\text{O}_2$; peptide 154–160 [see Table S4]). As such, this analysis was only semiquantitative.

Quantification of capsid protein degradation. The proportion of undamaged capsid protein (CP/CP_0) was determined by the product of the intact fractions of the individual peptides ($\text{cp}_i/\text{cp}_{i,0}$) (equation 6):

$$\text{CP}/\text{CP}_0 = (\Pi \text{cp}_i/\text{cp}_{i,0}) \quad (6)$$

The capsid protein degradation rate constant (k_{CP}) was calculated for all treatments except ClO_2 according to a first-order model versus disinfectant dose (equation 7):

$$\ln \frac{\text{CP}}{\text{CP}_0} = -k_{\text{CP}} C_d t \quad (7)$$

For ClO_2 , protein degradation was described by a Hom-type model (equation 8):

$$\ln \frac{\text{CP}}{\text{CP}_0} = -k_{\text{CP},H} C_d^n t^{m-1} \quad (8)$$

where $k_{\text{CP},H}$ is the Hom protein degradation rate constant [$(\text{mg liter}^{-1} \text{s}^{m-1})^{-1}$], n is the dilution coefficient (set to 1 in accordance with inactivation experiments), and m is the constant for the inactivation rate law, which describes the deviation from the ideal first-order model (equation 7). The ClO_2 concentration varied over time, due to autodecomposition and evaporation. ClO_2 has been reported to degrade exponentially as follows (equation 9) (31):

$$C_d = C_{d,0} e^{-k_{\text{ClO}_2} t} \quad (9)$$

where $C_{d,0}$ and C_d are the chlorine dioxide concentration at times 0 and t (s), respectively, and k_{ClO_2} is the first-order ClO_2 decay rate constant. Recall that the ClO_2 experiments for protein damage assessment were conducted in sacrificial reactors at different initial ClO_2 concentrations. The integration of equation 9 over time thus provided the respective ClO_2 dose for each reactor. The average C_d in each reactor (input parameter for the Hom model) was then obtained by dividing the dose by the time of exposure, t . The parameters for the Hom model were fitted in Sigmaplot (version 12.0, 2011).

To determine if protein degradation differed among the three viruses and from zero, rate constants were compared by ANCOVA, whereby a P value of < 0.05 was deemed significant.

Computational modeling of methionine oxidation in MS2. The free energy difference for the reaction of oxidation of Met88 by $^1\text{O}_2$ in fr and MS2 was evaluated by combined molecular dynamics and thermodynamic integration simulations using the NAMD package (32). The Amber force field (parm10) (AMBER 11; D. A. Case et al., University of California, San Francisco) was used to describe the protein environment, while additional parameters required for the methionine sulfoxide residue were generated using the Gaussian 03 (M. Frisch et al., Gaussian Inc., Walling-

TABLE 1 Inactivation rate constants (\pm standard errors) for each virus and each disinfectant^a

Bacteriophage	$\text{UV}_{254}, k_{\text{CW}}$ [(J m ⁻²) ⁻¹]	$^1\text{O}_2, k_{\text{CW}}$ [(mg liter ⁻¹ s) ⁻¹]	FC, k_{CW} [(mg liter ⁻¹ s) ⁻¹]	ClO_2, k_H [(mg liter ⁻¹ s ^{m-1}) ⁻¹]
MS2	$8.6 \times 10^{-3} \pm 1.1 \times 10^{-3}$	$1.5 \times 10^4 \pm 0.3 \times 10^3$	$1.3 \times 10^{-1} \pm 0.1 \times 10^{-1}$	$3.7 \pm 0.1, m = 1.46 \pm 0.01$
fr	$9.5 \times 10^{-3} \pm 1.1 \times 10^{-3}$	$2.0 \times 10^4 \pm 0.3 \times 10^3$	$1.3 \times 10^{-1} \pm 0.1 \times 10^{-1}$	$3.3 \pm 0.5, m = 1.35 \pm 0.03$
GA	$9.6 \times 10^{-3} \pm 1.0 \times 10^{-3}$	$1.6 \times 10^4 \pm 0.3 \times 10^3$	$1.3 \times 10^{-1} \pm 0.1 \times 10^{-1}$	$14.2 \pm 1.1, m = 1.31 \pm 0.02$

^a Statistically significant differences in inactivation were found for the combinations indicated: UV_{254} , GA-MS2 ($P = 0.027$); $^1\text{O}_2$, MS2-fr ($P < 0.001$), MS2-GA ($P = 0.022$), fr-GA ($P < 0.001$); ClO_2 , MS2-fr ($P = 0.026$), MS2-GA ($P = 0.007$), fr-GA ($P = 0.001$).

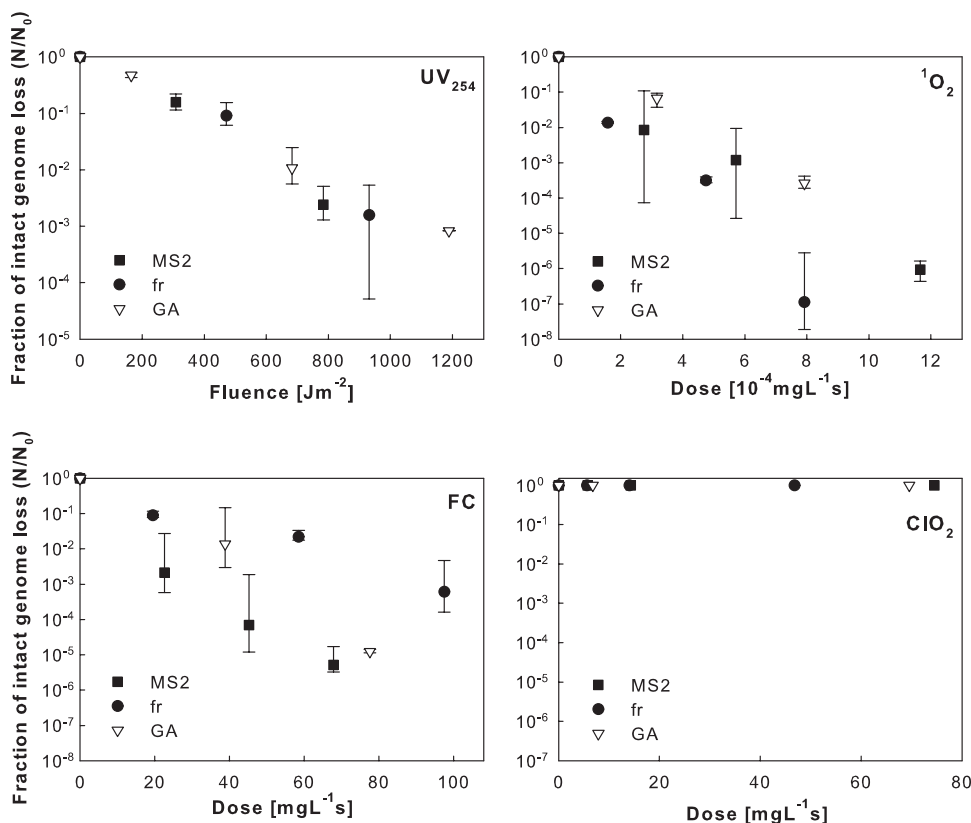


FIG 3 Comparison of levels of genome damage to the three phages upon inactivation by the four disinfectants investigated. Statistically significant differences in genome degradation were found for the combinations indicated: 1O_2 , fr-MS2 ($P = 0.029$), fr-GA ($P = 0.005$); FC, MS2-fr ($P = 0.006$), fr-GA (0.011). Genome degradation upon exposure to ClO_2 was not different from zero.

ford, CT) quantum mechanical software package and the restrained electrostatic potential (RESP) procedure for the point electrostatic charges and the General Amber Force Field (33) for the remaining parameters. Pressure was set to 100 kPa, and the temperature was set to 300 K. Additional details are given in the supplemental material.

Poisson-Boltzmann calculations were performed to investigate the stability of the capsid at different ionic strengths. Ion charges of 1 and -1 with radii of 2 Å were used, and the biomolecule and solvent dielectric constants were set to 2 and 78, respectively. Additional details are given in the supplemental material.

The solvent-accessible surface area (SASA) for the MS2 and fr sulfur atoms was calculated using VMD (34). Each reported SASA is an average of 10 SASAs obtained using the structures extracted for the adaptive Poisson-Boltzmann solver (APBS) calculations. The probe radius was set to 1.4 Å.

RESULTS

Comparison of inactivation kinetics. Inactivation kinetics for each virus upon treatment by the different disinfectants are shown in Fig. 1. Inactivation by UV₂₅₄, 1O_2 , and FC was first order with respect to dose (equation 1). For ClO_2 , in contrast, inactivation deviated from first order and exhibited significant tailing at higher doses. Consequently, inactivation rate constants for ClO_2 were determined by a fit to the Hom model (equation 2).

The inactivation rate constants for all treatments are summarized in Fig. 2, and the exact values and associated uncertainties are listed in Table 1. For free chlorine, the inactivation rate constants did not significantly differ between the three viruses. In

contrast, for UV₂₅₄ a significantly higher rate constant was found for GA than for MS2 ($P = 0.027$). For singlet oxygen and ClO_2 , all three viruses were inactivated at different rates: for ClO_2 , the sequence of inactivation in the initial, linear part of the inactivation curve followed the order fr < MS2 < GA ($P = 0.026$ for MS2 versus fr; $P = 0.007$ for MS2 versus GA; $P = 0.001$ for fr versus GA), whereas for singlet oxygen, the order was MS2 < GA < fr ($P < 0.001$ for MS2 versus fr; $P = 0.022$ for MS2 versus GA; $P < 0.001$ for fr versus GA).

Comparison of levels of genome degradation. Genome degradation as a function of disinfectant dose is shown in Fig. 3. This representation illustrates the genome-damaging capacity of a specific treatment, as well as the differences between each virus. The corresponding experimental degradation rate constants are summarized in Fig. 2 and Table 2. UV₂₅₄, FC, and 1O_2 were all capable of degrading the genome in each virus. Only subtle differences were observed among the three viruses: for UV₂₅₄, genome degradation proceeded at the same rate for all viruses; upon treatment by 1O_2 , the fr genome degraded slightly faster than the MS2 ($P = 0.029$) and GA ($P = 0.005$) genomes, and the opposite was found for free chlorine, which degraded the fr genome more slowly than it did the MS2 ($P = 0.006$) and GA ($P = 0.011$) genomes. Notably, ClO_2 did not induce measurable genome damage in any of the viruses.

To measure the importance of genome damage as a mechanism of inactivation, the extent of genome damage was directly

TABLE 2 Genome and protein degradation rate constants (\pm standard errors) for each virus and each disinfectant^a

	UV ₂₅₄			¹ O ₂			FC			ClO ₂		
	Bacteriophage	Genome (<i>k</i> _G) [J m ⁻²] ⁻¹	Protein vs dose (<i>k</i> _{CP}) [J m ⁻²] ⁻¹	Genome (<i>k</i> _G) [mg liter ⁻¹ s] ⁻¹	Protein vs dose (<i>k</i> _{CP}) [mg liter ⁻¹ s] ⁻¹	Genome (<i>k</i> _G) [mg liter ⁻¹ s] ⁻¹	Protein vs dose (<i>k</i> _{CP}) [mg liter ⁻¹ s] ⁻¹	Genome (<i>k</i> _G) [mg liter ⁻¹ s ^{m-1}] ⁻¹	Protein vs dose (<i>k</i> _{CP,fit}) [mg liter ⁻¹ s ^{m-1}] ⁻¹			
MS2		7.7 × 10 ⁻³ ± 1.4 × 10 ⁻³	2.5 × 10 ⁻⁴ ± 0.2 × 10 ⁻⁴	1.1 × 10 ⁴ ± 0.2 × 10 ⁴	1.7 × 10 ² ± 0.3 × 10 ²	1.7 × 10 ⁻¹ ± 0.3 × 10 ⁻¹	5.2 × 10 ⁻² ± 0.2 × 10 ⁻²	NS	2.1 ± 0.7, <i>m</i> = 1.7 ± 0.1			
fr		7.5 × 10 ⁻³ ± 1.6 × 10 ⁻³	2.7 × 10 ⁻⁴ ± 0.5 × 10 ⁻⁴	2.0 × 10 ⁴ ± 0.2 × 10 ⁴	NS	6.9 × 10 ⁻² ± 1.4 × 10 ⁻²	6.1 × 10 ⁻² ± 0.8 × 10 ⁻²	NS	1.0 ± 0.5, <i>m</i> = 1.8 ± 0.1			
GA		6.1 × 10 ⁻³ ± 0.7 × 10 ⁻³	NS	1.3 × 10 ⁴ ± 0.2 × 10 ⁴	NS	1.5 × 10 ⁻¹ ± 0.2 × 10 ⁻¹	6.4 × 10 ⁻² ± 0.4 × 10 ⁻²	NS	3.7 ± 0.4, <i>m</i> = 1.5 ± 0.1			

^a NS indicates nonsignificant decay. Statistically significant differences in genome degradation were found for the combinations indicated: ¹O₂, fr-MS2 ($P = 0.029$), fr-GA ($P = 0.005$); FC, MS2-fr ($P = 0.006$), fr-GA (0.011). Genome degradation upon exposure to ClO₂ was not different from zero.

compared to inactivation (Fig. 4). Three possibilities exist. (i) If N/N_0 is $< C_v/C_{v,0}$ (slope of genome degradation versus inactivation in Fig. 4 < 1), there is more virus inactivation than genome damage, and therefore, genome damage can only partially contribute to the overall inactivation. In this scenario, some population of inactivated viruses must contain intact genomes. (ii) If N/N_0 is equal to $C_v/C_{v,0}$ (slope in Fig. 4 = 1), there is sufficient genome damage to fully account for the loss of infectivity, assuming that each genome lesion causes inactivation (single-hit model). (iii) If N/N_0 is $> C_v/C_{v,0}$ (slope in Fig. 4 > 1), then infective viruses with damaged genomes are present. This implies that the virus can sustain multiple genome lesions before becoming inactivated.

As can be readily seen in Fig. 4, genome damage could not fully account for inactivation of any virus by ClO₂ (slope < 1). In addition, three further virus-disinfectant combinations yielded less genome damage than inactivation: fr-FC ($P = 0.004$), GA-UV₂₅₄ ($P = 0.003$), and GA-¹O₂ ($P = 0.033$). For these combinations of virus and disinfectant, protein degradation must therefore play a role in the inactivation process. For the remaining virus-disinfectant pairs, the extent of inactivation corresponded to that of genome degradation (slope = 1). No virus-disinfectant combination yielded an obvious multihit scenario (slope > 1).

Comparison of capsid protein degradation. Figure 5 shows capsid protein degradation as a function of disinfectant dose for all viruses and disinfectants. The corresponding rate constants are summarized in Fig. 2, and the exact values as well as their associated errors are listed in Table 2. For the viruses that exhibited significant protein degradation by UV₂₅₄, ¹O₂, or FC, protein degradation followed first-order kinetics with respect to disinfectant dose. ClO₂, in contrast, caused tailing with increasing dose, similar to the corresponding inactivation curves (Fig. 1). However, if analyzed as a function of inactivation (Fig. 6), capsid protein degradation by ClO₂ also followed a first-order model.

The effects of UV₂₅₄ and singlet oxygen on the capsid proteins were generally subtle. Upon treatment by UV₂₅₄, only MS2 and fr sustained a statistically significant amount of capsid protein damage, while GA's capsid protein remained unaffected. Singlet oxygen caused slight, but significant, damage to MS2 only. Free chlorine as well as ClO₂, in contrast, rapidly degraded the capsid proteins of all viruses. Upon exposure to the same dose, free chlorine acted more efficiently on the GA capsid than on MS2 ($P = 0.007$), though the degradation rate constants differed by a factor of only 1.2. If analyzed as a function of inactivation, however, the three virus capsids degraded at indistinguishable rates (Fig. 6). Finally, chlorine dioxide treatment exhibited significantly different degradation rate constants for fr and GA ($P < 0.01$).

Identification of susceptible capsid protein domains. To identify and compare the susceptible capsid domains for each combination of virus and disinfectant, we monitored the degradation of individual protein regions (peptides) of the capsid protein during disinfection. A summary of the resulting peptide degradation rate constants is shown in Fig. 7. The effect of UV₂₅₄ and ¹O₂ on the different peptides was small, whereas FC and ClO₂ caused extensive degradation. While ClO₂ caused damage to selected peptides only, FC was less specific and reacted with all parts of the capsid.

Among the three viruses, subtle differences in the damage pattern could be observed. For MS2, at least one peptide was degraded by each disinfectant: UV₂₅₄ mainly affected peptides

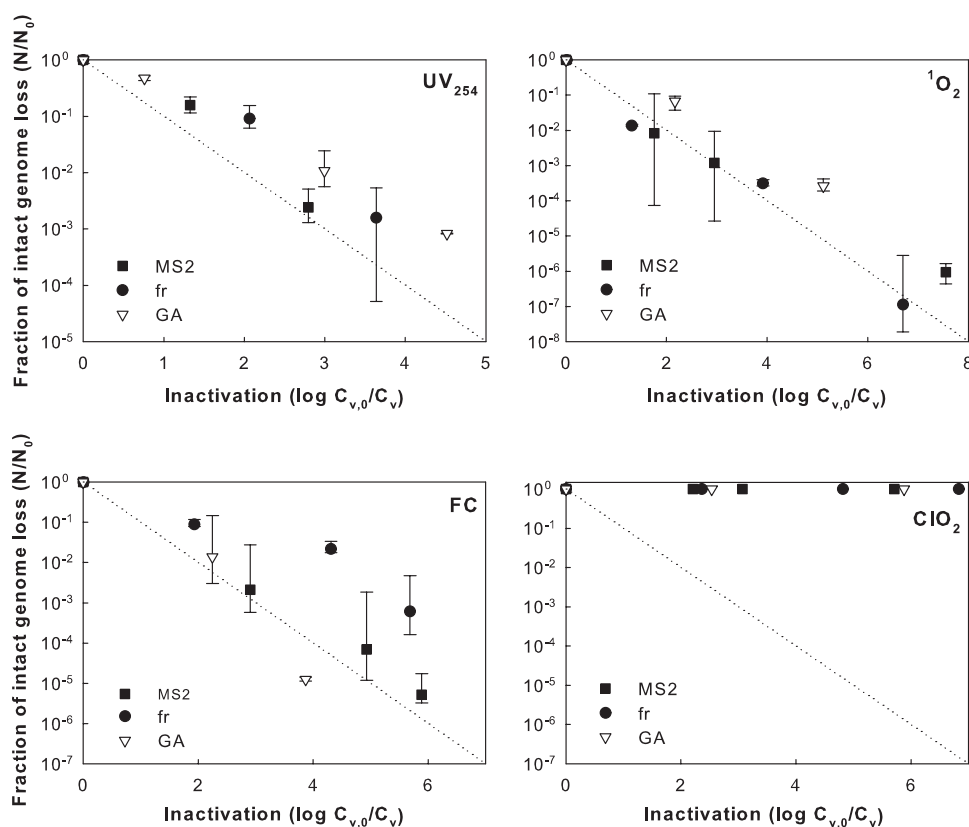


FIG 4 Comparison of genome damage and virus inactivation of the three bacteriophages upon inactivation by the four disinfectants. The dotted line represents a 1:1 relation between inactivation and genome degradation. Besides ClO_2 , which did not induce genome damage, significantly slower genome degradation than inactivation was observed for the following combinations: fr-FC ($P = 0.004$), GA- UV_{254} ($P = 0.003$), and GA- $^1\text{O}_2$ ($P = 0.033$).

44–49 and 114–129, singlet oxygen selectively degraded peptide 84–106, ClO_2 degraded peptide 84–106 and the adjacent peptide 59–82, and free chlorine affected all peptides. The fr damage pattern was very similar to that observed for MS2, although peptide 84–106 was not degraded by singlet oxygen. Finally, GA did not sustain any measurable peptide degradation by UV_{254} or singlet oxygen.

MALDI analysis of the undigested capsid protein revealed instances of protein backbone cleavage after treatment by UV_{254} and free chlorine (see Fig. S6 in the supplemental material). For these two disinfectants, protein degradation could thus be attributed to both protein backbone cleavage and modifications of the amino acid side chains. UV_{254} induced only backbone cleavage in MS2 and fr. In both cases, a single cleavage occurred around residues Cys46 and Ser47, consistent with the observed loss of peptide 44–49 (Fig. 7). Treatment by FC led to capsid protein fragmentation in all three viruses at various locations. Among the observed fragmentation products, a dominant fragment resulted from cleavage between residues 50 and 51 in all three viruses (see Fig. S6). Specifically, the main cleavage products detected after FC treatment had masses of 5,280, 5,335, and 5,258 Da for MS2, fr, and GA, respectively; the predicted mass of peptide 1–50 corresponds to 5,278 Da for MS2, 5,335 Da for fr, and 5,254 Da for GA. Singlet oxygen and ClO_2 did not result in measurable backbone cleavage. Protein degradation by these two disinfectants was thus mainly attributed to modification of the side chains.

Identification of susceptible A protein domains. In addition to the capsid protein, the degradation of the A protein was analyzed in GA after treatment by UV_{254} and $^1\text{O}_2$. Despite the low MALDI coverage, it was evident that both UV_{254} and $^1\text{O}_2$ caused the A protein to degrade (see Fig. S7 in the supplemental material); peptides 42–51 and 172–183 were damaged by UV_{254} , and peptide 56–65 degraded during $^1\text{O}_2$ treatment.

MS/MS identification of amino acids modified by singlet oxygen. The capsid protein peptide analysis (Fig. 7) showed that in MS2 only one peptide was degraded by singlet oxygen, and a single product with a mass shift of +16, corresponding to an oxidation event, was generated. MS/MS analysis was performed on this product and revealed that residue Met88 was oxidized (see Fig. S8 in the supplemental material). Because GA does not contain any methionine residues, no corresponding product formed. Interestingly, however, this product also did not form in fr despite the fact that it does contain Met88.

Computational rationalization of singlet oxygen findings. To explain the absence of Met88 oxidation by $^1\text{O}_2$ in fr, this residue was compared to the corresponding residue in MS2 using a range of computational tools. Three factors were considered: the energy cost associated with the oxidation process, the strength of intracapsid binding (i.e., binding between capsid protein triplets), and the solvent-accessible surface area (SASA) surrounding the Met88 residue. Thermodynamic integration revealed that the two viruses had similar free energy of oxidation costs of approximately 4 kcal/mol (see Table S5 in the supplemental material). APBS

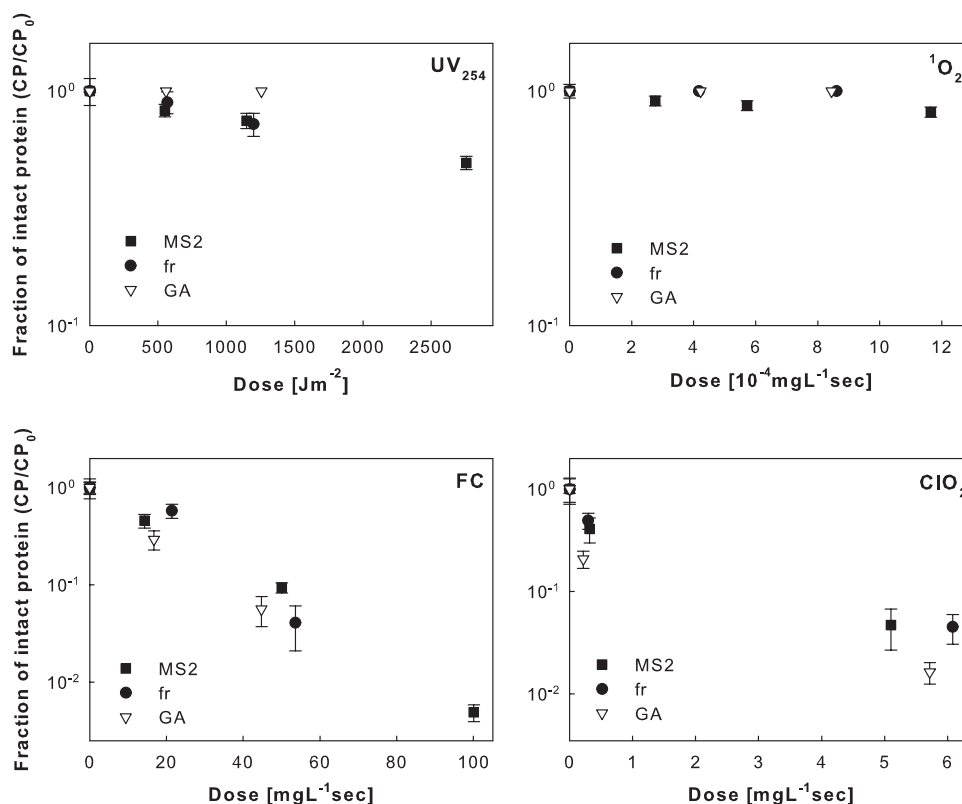


FIG 5 Comparison of capsid protein damage versus disinfectant dose between the three viruses upon inactivation by the four disinfectants. Error bars represent the standard errors. Statistically significant differences in protein degradation were found for the combinations indicated: FC, MS2-GA ($P = 0.007$); ClO₂, fr-GA ($P < 0.01$).

calculations (see Table S6) showed that both shared similar electrostatic components to intracapsid binding. Calculating the SASA using the sulfur atoms of Met88 (highlighted in Fig. 8a and b), however, showed a marked difference between MS2 and fr. The SASA for MS2 was measured to be $1.6 \pm 0.2 \text{ \AA}^2$ while the SASA for fr was only $0.4 \pm 0.2 \text{ \AA}^2$. This difference is illustrated in Fig. 8c and d, where representative structures used to calculate the SASAs are shown.

DISCUSSION

Influence of genome and protein composition on degradation and inactivation. Our data indicate that, despite their (small) differences in composition, all three viruses were affected by the disinfectants in roughly the same way: genome damage was strong for inactivation by UV₂₅₄, FC, and ¹O₂ and not measurable for chlorine dioxide (Fig. 3); capsid protein degradation was subtle for UV₂₅₄ irradiation and singlet oxygen treatment and extensive for chlorine dioxide and FC.

Genome degradation may be related to genome length, nucleotide content, and genome structure. More specifically, longer genomes offer more targets for attack, higher contents of guanine (the most easily oxidizable nucleobase) (see Table S7 in the supplemental material) may increase the susceptibility to oxidants, and genome structure may dictate the accessibility of oxidants to the reactive sites. The genome lengths and contents of the three phages used herein were similar, with expected differences in genome degradation of no more than 10% (based on genome length and nucleotide reactivity) (see Tables S7 and S8). This is consis-

tent with our findings, in which only small differences in the genome degradation rates were observed among the three viruses and UV₂₅₄, ¹O₂, and FC treatments.

A more complex situation is encountered for protein degradation. As for the genome, protein composition, length, and structure are likely to influence degradation. Based on amino acid reactivity (see Table S7 in the supplemental material), significantly slower protein degradation was expected for GA than for the two other viruses. This is due to the fact that MS2 and fr capsid proteins contain two cysteines and two methionines, the two amino acids most reactive toward oxidants (see Table S7), whereas the GA capsid protein has neither. As such, the absence of cysteine and methionine implies that the capsid protein of GA may degrade more slowly than those of MS2 and fr upon disinfection by oxidants. Experimentally, however, the extents of capsid protein damage were similar for all three viruses (Fig. 5 and 6). This suggests that the composition of the viral protein is not the most important factor governing its degradation, but that protein structure may also play an important role. For example, studies have shown that despite their high reactivity, cysteines in bacteriophage f2, a virus similar to the ones investigated here, were not degraded by ClO₂ due to their poor accessibility (35).

Our findings regarding the extent of genome and protein degradation provide some preliminary conclusions regarding the prevailing disinfection mechanisms. First, the main target of UV₂₅₄ and ¹O₂ is the genome, which may result in the inability of a virus to replicate. Free chlorine can target both genome and proteins,

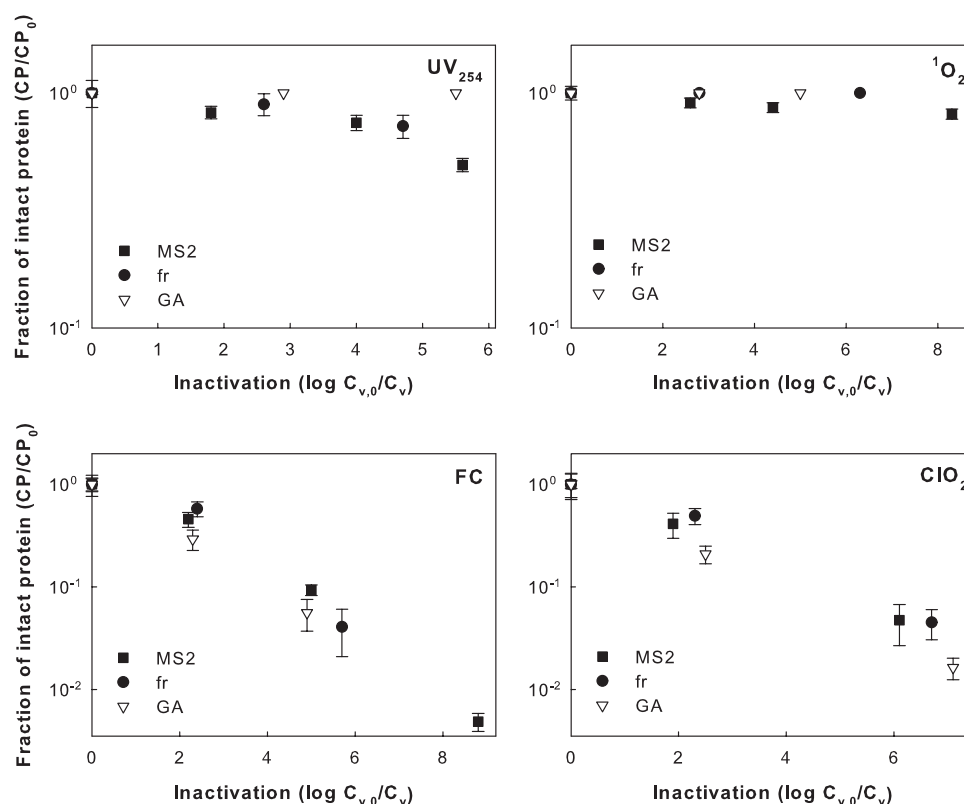


FIG 6 Protein degradation per log inactivation. Error bars represent standard errors. Statistically significant differences in protein degradation were found for the combinations indicated: UV₂₅₄, MS2-fr ($P = 0.038$); ClO₂, fr-GA ($P = 0.027$).

leading to a loss in replication, as well as protein-mediated functions involved in infection (i.e., host attachment and genome injection into the host). Viruses disinfected by ClO₂ may retain the ability to replicate but cannot penetrate the host cell. Overall, these findings are consistent with previous work (28), in which the loss of the individual functions of MS2 upon disinfection were investigated. Interestingly, however, the subtle differences in genome and protein composition of fr and GA compared to MS2 were nevertheless sufficient to cause some alterations in the prevailing inactivation mechanisms. In the following paragraphs, the observed trends are discussed for each disinfectant individually.

UV₂₅₄. Uracil dimers are the main product following RNA irradiation by UV₂₅₄ (36); hence, adjacent uracils are the genome feature most prone to degradation by UV₂₅₄. Among the three viruses, GA contains the most adjacent uracils (see Table S7 in the supplemental material), and hence, the GA genome is expected to degrade most rapidly. The experimental findings, however, show that inactivation by UV₂₅₄ caused no significant difference in the extent of genome damage among the three viruses (Fig. 3; Table 2). This thus suggests that the composition of the genome is not the only factor determining its degradation rate. Instead, the secondary and tertiary structure of the genome may also influence its degradation.

Given that the genome is the main target of UV₂₅₄, inactivation of the three phages was expected to be directly related to their extent of genome damage. However, despite their similar extents of genome damage, GA was inactivated more rapidly than MS2 (Fig. 1 and 2; Table 1). In addition, its genome damage was insuff-

ficient to account for inactivation (Fig. 2 and 4), indicating that protein damage must contribute to the inactivation of GA.

Several aromatic amino acids can be affected by UV₂₅₄ irradiation (see Table S7 in the supplemental material), yet only little degradation of peptides containing these residues was observed (Fig. 7). This can be explained by the nucleotides' greater sensitivity to degradation by UV₂₅₄ compared to that of amino acids (see Table S7), which implies that the three viruses were inactivated by genome degradation before substantial damage to aromatic amino acids in the capsid protein could accumulate. For MS2 and fr, however, slight capsid degradation was observed in peptide 44–49, which contains no UV₂₅₄-susceptible amino acids (Fig. 7). In previous work (37), it was shown that the degradation of peptide 44–49 in MS2 was caused by backbone cleavage around amino acids Cys46 and Ser47. This cleavage event was facilitated by the presence of both RNA and cysteine at the cleavage site. fr also contains the relevant cysteine in its capsid protein, whereas in GA this cysteine is absent. Consequently, cleavage at the same site was found for fr but not for GA (see Fig. S6). The cleavage event is thought to contribute to MS2 inactivation by preventing it from injecting its genome into the host (28). Besides genome degradation, capsid cleavage thus contributes to a small extent to the inactivation of MS2, and presumably fr, while this mechanism is not present in GA.

Since neither genome degradation nor capsid protein cleavage could account for the inactivation of GA by UV₂₅₄, GA's inactivation must involve a relevant contribution of the A protein. Consistent with this hypothesis, significant degradation of the A pro-

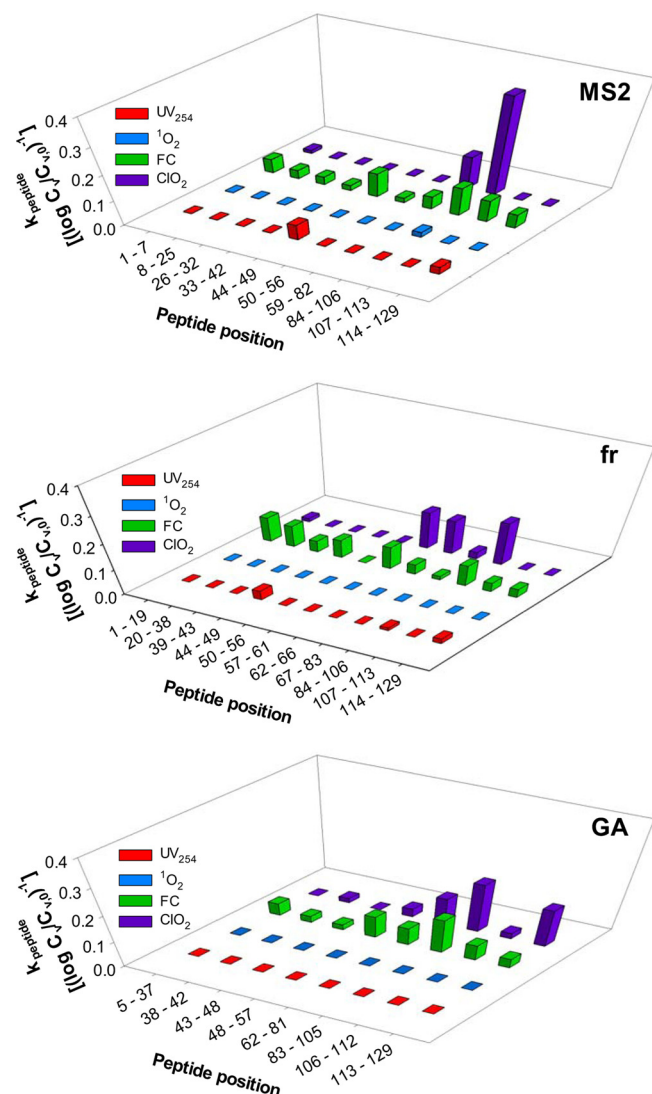


FIG 7 Degradation rate constants k_{peptide} for the individual peptides within the capsid proteins of the three viruses. Rate constants were calculated according to equation 5. The numbers on the x axis correspond to the positions of the peptides.

tein was observed (see Fig. S7 in the supplemental material). Furthermore, it cannot be excluded that the viruses underwent protein modifications, which are not measurable with the methods used here, such as structural changes that inhibit the virus from binding to its host.

Singlet oxygen. For singlet oxygen, damage to the genome (oxidative genome lesions [18, 28] and RNA-protein cross-links [38]) has been identified as the main inactivating factor. Therefore, inactivation was expected to follow the same trend as genome degradation. Based on genome composition, fr should exhibit faster genome degradation and hence faster inactivation than GA or MS2, since its genome contains the greatest number of easily oxidizable guanines (see Table S8 in the supplemental material). This was seen to some extent in our results; indeed, fr did exhibit faster genome decay than did GA and MS2 (Fig. 2 and 3; Table 2), though comparison with MS2 did not yield a statistically significant difference. Correspondingly, inactivation was faster for fr

than for MS2 and GA (Fig. 1 and 2; Table 1). Differences in genomic content among the three viruses may thus be responsible for the observed inactivation rate differences.

The extent of genome degradation in fr and MS2 roughly corresponded to its extent of inactivation by $^1\text{O}_2$ ($N/N_0 = C_v/C_{v,0}$), but genome degradation in GA was too small to account for inactivation ($N/N_0 < C_v/C_{v,0}$) (Fig. 2 and 4). This discrepancy could not be explained by contribution of the capsid protein to inactivation, since GA's capsid remained unaffected by this disinfection method. Similar to what was observed with UV_{254} , GA's inactivation by $^1\text{O}_2$ must therefore involve a significant contribution of the A protein. Indeed, A protein analysis revealed degradation of peptide 56–65, which contain $^1\text{O}_2$ -susceptible residues tryptophan and tyrosine (see Fig. S7 and Table S4 in the supplemental material). Only a small part of the A protein was analyzed; it is, however, likely that unanalyzed parts of the protein also degrade, as was previously observed for MS2 (28). Furthermore, singlet oxygen is known to cause protein cross-linkages (16), which may not be detected with the methods used here but may further contribute to inactivation.

In MS2, $^1\text{O}_2$ caused oxidation of the capsid protein Met88 residue (Fig. 7; see also Fig. S8 in the supplemental material). Interestingly, fr's capsid protein Met88 was not affected by $^1\text{O}_2$. From a thermodynamic standpoint (see Table S5), if MS2's Met88 is oxidized, then fr's Met88 should also be oxidized. Furthermore, the magnitude of binding energy between capsid triplets was found to be similar, and the electrostatic component of the MS2 intracapsid binding energy was even slightly stronger than that of fr (see Table S6); therefore, the observed Met88 oxidation difference was not due to differences in capsid stability. An explanation could be found, however, by considering the solvent-accessible surface area (SASA) of the Met88 sulfur atoms, which did show a marked difference between MS2 and fr. The SASA for fr was measured to be four times smaller than that of MS2 (Fig. 8c and d). The difference in SASA is attributed primarily to the position of the Leu90 residue (see Fig. S9), which allows the region surrounding the sulfur of Met88 to more easily accommodate a $^1\text{O}_2$ atom in MS2 than the same region in fr. The residues within 5 Å of the sulfur atom of Met88 for both capsid proteins are shown in Fig. 8e and f. In both cases, the protein surrounding the sulfur atoms is hydrophobic, a more amenable environment to $^1\text{O}_2$ than water. In addition, water exhibits a slightly higher penetration of the capsid structure of fr than that of MS2 (see Fig. S10).

Our calculations thus indicate that in the vicinity of Met88, $^1\text{O}_2$ can have faster diffusion kinetics in MS2 than in fr due to both a larger accessible space and smaller hindrance originating from buried waters that must be displaced to access the Met88 site. We note here that the local environment and accessibility to a specific site have been reported as being crucial elements in accounting for protein reactivity toward $^1\text{O}_2$ (39).

Free chlorine. Our previous results showed that FC caused extensive genome damage but that inactivation was also accompanied by significant protein damage (28). Other reports suggest that genome damage is entirely responsible for inactivation by FC (9, 40). The findings here confirm that FC caused extensive genome damage in all three phages. However, the fr genome was found to degrade slower than the GA and MS2 genomes (Fig. 2 and 3; Table 2). This finding was surprising for two reasons: first, the high guanine content of fr should make it the most reactive, and second, another oxidant, $^1\text{O}_2$, reacted fastest with the fr ge-

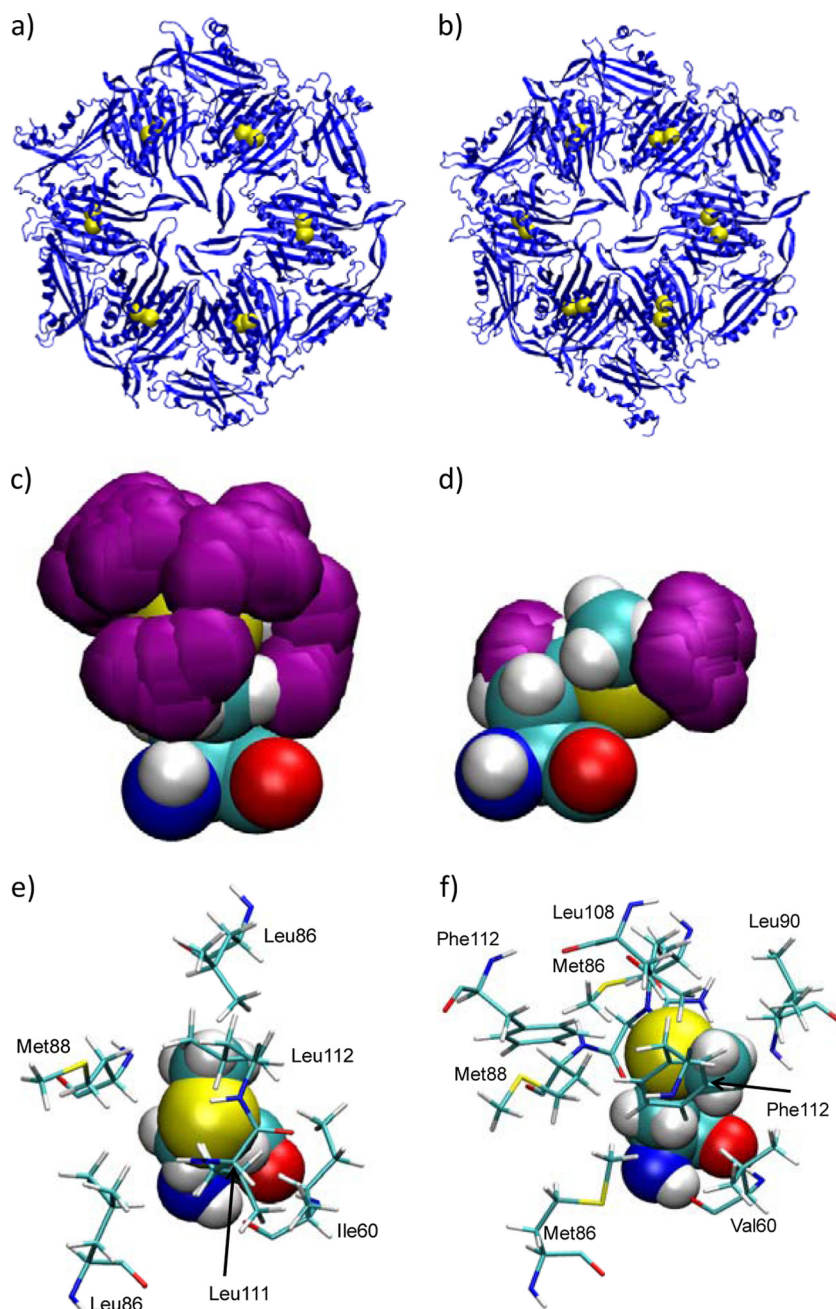


FIG 8 (a and b) Plan views of fragments of the MS2 (a) and fr (b) capsid where each fragment contains six copies of the triplet. The sulfur atoms of the Met88 are shown as yellow spheres. (c and d) Purple spheres represent the SASA of one of the 12 Met88 residues used to calculate the SASA for MS2 (c) and fr (d). The images show the accumulation of 10 equidistant snapshots taken from simulations of 2-ns duration. The surrounding protein is not shown so as to aid clarity. The oxygen atoms are colored red, nitrogens are blue, carbons are cyan, sulfurs are yellow, and hydrogens are white. (e and f) Residues within 5 Å of the sulfur atom of the Met88 chain A for MS2 (e) and fr (f), where Met88 is shown in the space-filling VDW representation and the surrounding residues are shown in licorice representation.

nome. These arguments support the conclusion that structural features of the RNA have varied impacts on different oxidants.

Regardless of their different genome degradation rates, the three bacteriophages inactivated at similar rates (Fig. 1 and 2; Table 1). This is consistent with our previous findings for MS2 (28) that despite the major role of genome degradation, inactivation is in part controlled by a protein component. Indeed, free chlorine-induced capsid protein damage was extensive for all

three viruses (Fig. 5 and 6). The strong and slightly variable effects of FC on the capsid proteins are in agreement with our finding that all three viruses were inactivated by FC at the same rate (Fig. 1 and 2). In other words, even though the viruses incurred different inactivating events, the overall damage to genomes and proteins resulted in similar inactivation rates.

The peptide degradation pattern (Fig. 7) shows that compared to the other treatments, degradation of proteins by free chlorine

treatment was less specific. The relatively homogeneous distribution of damage in the various regions of the capsid protein is due to FC's ability not only to react with amino acid side chains but also to cleave protein backbones (see Fig. S6 and Table S7 in the supplemental material). Nevertheless, the peptides most readily degraded tended to contain FC-susceptible residues (methionine, cysteine, and tryptophan) (e.g., peptides 84–106, 107–113, and 44–49 in MS2), whereas the peptides lacking susceptible residues were more resistant to FC (e.g., peptides 50–56, 39–43, and 107–113 in fr).

Chlorine dioxide. Inactivation by ClO_2 did not lead to quantifiable genome degradation (Fig. 3), confirming our previous results and other reports that the mechanism of bacteriophage inactivation is entirely protein dependent (2, 28, 35). The lack of genome damage is surprising given that the rather small size of the chlorine dioxide molecule should allow it to penetrate the virus capsid by way of the 1- to 2-nm pores in the capsid and to access the genome. The absence of genome damage may be explained by the fact that chlorine dioxide reacts more rapidly with some amino acids than with nucleotides (e.g., tryptophan reacts at least 75 times faster than the most susceptible nucleotide, G [11, 41]) (see Table S7 in the supplemental material). Hence, by the time detectable genome damage has accumulated, the virus may have already been inactivated as a result of protein damage.

As expected, extensive capsid protein degradation was observed after chlorine dioxide exposure (Fig. 5 and 6). Protein degradation was fastest for GA, which corresponds to the order of observed inactivation rates (Fig. 1 and 2). This suggests that virus inactivation is governed by capsid protein degradation, a point that is further supported by the fact that capsid protein degradation was directly proportional to inactivation (Fig. 6).

The peptide results (Fig. 7) showed a pattern of localized degradation with the majority of capsid protein degradation occurring between amino acids 61 and 106. Interestingly, not all of the peptides in this region contained amino acids susceptible to ClO_2 (see Table S7 in the supplemental material). Their degradation can be explained by the fact that ClO_2 is a one-electron acceptor that can create radicals upon reaction (41). This can trigger radical chain reactions that damage adjacent parts of the protein, as has been observed previously with hydroxyl radicals (42). Spatially, the affected regions are located around the pores and then propagate to the inside space between the pores (see Fig. S11).

Implications for estimating virus disinfection kinetics. In conclusion, this study illustrates the complexity involved in predicting virus inactivation. Depending on the disinfectant, the three related viruses exhibited equal, similar, or very different inactivation rates. Furthermore, the relative susceptibilities of the three viruses varied with the different disinfectants. This could be explained by differences in both the mode of action of the four inactivating treatments and the inactivation mechanisms among the viruses.

For treatments with a strong genome-damaging component (UV_{254} , $^1\text{O}_2$, and FC), inactivation kinetics were generally similar among the three phages (Fig. 1 and 2; Table 1). In contrast, the protein-damaging ClO_2 led to much greater differences in inactivation. This finding leads to the hypothesis that it may be possible to predict the inactivation kinetics of experimentally nontractable viruses based on related species, as long as the disinfectant is primarily targeting the genome. On the other hand, if a protein component is involved, such predictions are not likely to be accurate. We caution, however, that this hypothesis remains to be tested

with greater sets of related viruses. In particular, it may be valid only for viruses with similar genome lengths, such as the three species studied here.

To allow for accurate predictions of virus inactivation, good knowledge of the dominant disinfection mechanisms is thus essential. This may include better information on the disinfectants' mode of action and a comprehensive understanding of the effect of composition and structure on genome and protein reactivity. Finally, it would be desirable to know the relevant virus domains involved in the infectious cycle, in particular host attachment sites. This would enable more conclusive statements of the impact of protein degradation on inactivation and would allow a more targeted analysis.

ACKNOWLEDGMENTS

This work was supported by the Swiss National Fund (project number CRS122_127568/1). This work was granted access to the HPC resources of JADE based in France at the Centre Informatique National de l'Enseignement Supérieur made available within the Distributed European Computing Initiative by the PRACE-2IP, receiving funding from the European Community's Seventh Framework Programme (FP7/2007–2013) under grant agreement no. RI-283493.

We thank Satoshi Takahama for help with the statistical analysis.

REFERENCES

- Rodriguez-Lazaro D, Cook N, Ruggeri FM, Sellwood J, Nasser A, Nascimento MS, D'Agostino M, Santos R, Saiz JC, Rzezutka A, Bosch A, Girones R, Carducci A, Muscillo M, Kovac K, Diez-Valcarlos M, Vantarakis A, von Bonsdorff CH, Husman AMD, Hernandez M, van der Poel WHM. 2012. Virus hazards from food, water and other contaminated environments. *FEMS Microbiol. Rev.* 36:786–814.
- Lim MY, Kim JM, Ko G. 2010. Disinfection kinetics of murine norovirus using chlorine and chlorine dioxide. *Water Res.* 44:3243–3251.
- Engelbrecht RS, Weber MJ, Salter BL, Schmidt CA. 1980. Comparative inactivation of viruses by chlorine. *Appl. Environ. Microbiol.* 40:249–256.
- Simonet J, Gantzer C. 2006. Inactivation of poliovirus 1 and F-specific RNA phages and degradation of their genomes by UV irradiation at 254 nanometers. *Appl. Environ. Microbiol.* 72:7671–7677.
- Thurston-Enriquez JA, Haas CN, Jacangelo J, Gerba CP. 2005. Inactivation of enteric adenovirus and feline calicivirus by chlorine dioxide. *Appl. Environ. Microbiol.* 71:3100–3105.
- Kohn T, Nelson KL. 2007. Sunlight-mediated inactivation of MS2 coliphage via exogenous singlet oxygen produced by sensitizers in natural waters. *Environ. Sci. Technol.* 41:192–197.
- Park GW, Linden KG, Sobsey MD. 2011. Inactivation of murine norovirus, feline calicivirus and echovirus 12 as surrogates for human norovirus (NoV) and coliphage (F+) MS2 by ultraviolet light (254 nm) and the effect of cell association on UV inactivation. *Lett. Appl. Microbiol.* 52:162–167.
- Kahler AM, Cromeans TL, Roberts JM, Hill VR. 2011. Source water quality effects on monochloramine inactivation of adenovirus, coxsackievirus, echovirus, and murine norovirus. *Water Res.* 45:1745–1751.
- Li JW, Xin ZT, Wang XW, Zheng JL, Chao FH. 2002. Mechanisms of inactivation of hepatitis A virus by chlorine. *Appl. Environ. Microbiol.* 68:4951–4955.
- Alvarez ME, O'Brien RT. 1982. Mechanisms of inactivation of poliovirus by chlorine dioxide and iodine. *Appl. Environ. Microbiol.* 44:1064–1071.
- Napolitano MJ, Stewart DJ, Margerum DW. 2006. Chlorine dioxide oxidation of guanosine 5'-monophosphate. *Chem. Res. Toxicol.* 19:1451–1458.
- Eischeid AC, Meyer JN, Linden KG. 2009. UV disinfection of adenoviruses: molecular indications of DNA damage efficiency. *Appl. Environ. Microbiol.* 75:23–28.
- Kurosaki Y, Abe H, Morioka H, Hirayama J, Ikebuchi K, Kamo N, Nikaido O, Azuma H, Ikeda H. 2003. Pyrimidine dimer formation and oxidative damage in M13 bacteriophage inactivation by ultraviolet C irradiation. *Photochem. Photobiol.* 78:349–354.
- Wigginton KR, Menin L, Montoya JP, Kohn T. 2010. Oxidation of virus

- proteins during UV254 and singlet oxygen mediated inactivation. *Environ. Sci. Technol.* 44:5437–5443.
15. Eischeid AC, Linden KG. 2011. Molecular indications of protein damage in adenoviruses after UV disinfection. *Appl. Environ. Microbiol.* 77:1145–1147.
 16. Hotze EM, Badireddy AR, Chellam S, Wiesner MR. 2009. Mechanisms of bacteriophage inactivation via singlet oxygen generation in UV illuminated fullerol suspensions. *Environ. Sci. Technol.* 43:6639–6645.
 17. Pecson BM, Martin LV, Kohn T. 2009. Quantitative PCR for determining the infectivity of bacteriophage MS2 upon inactivation by heat, UV-B radiation, and singlet oxygen: advantages and limitations of an enzymatic treatment to reduce false-positive results. *Appl. Environ. Microbiol.* 75:5544–5554.
 18. Schneider JE, Phillips JR, Pye Q, Maitt ML, Price S, Floyd RA. 1993. Methylene-blue and Rose-Bengal photoinactivation of RNA bacteriophages—comparative studies of 8-oxoguanine formation in isolated RNA. *Arch. Biochem. Biophys.* 301:91–97.
 19. Baxter CS, Hofmann R, Templeton MR, Brown M, Andrews RC. 2007. Inactivation of adenovirus types 2, 5, and 41 in drinking water by UV light, free chlorine, and monochloramine. *J. Environ. Eng.* 133:95–103.
 20. Tars K, Bundule M, Fridborg K, Liljas L. 1997. The crystal structure of bacteriophage GA and a comparison of bacteriophages belonging to the major groups of *Escherichia coli* leviviruses. *J. Mol. Biol.* 271:759–773.
 21. Eaton AD, Clesceri LS, Rice EW, Greenberg AH (ed). 2005. Standard methods for the examination of water and wastewater, 21st ed. American Public Health Association, Washington, DC.
 22. Mattle MJ, Kohn T. 2012. Inactivation and tailing during UV254 disinfection of viruses: contributions of viral aggregation, light shielding within viral aggregates, and recombination. *Environ. Sci. Technol.* 46:10022–10030.
 23. Rahn RO. 1997. Potassium iodide as a chemical actinometer for 254 nm radiation: use of iodate as an electron scavenger. *Photochem. Photobiol.* 66:450–455.
 24. Gates D. 1998. The chlorine dioxide handbook. American Water Works Association, Denver, CO.
 25. Hoigne J, Bader H. 1994. Kinetics of reactions of chlorine dioxide (OClO) in water. 1. Rate constants for inorganic and organic-compounds. *Water Res.* 28:45–55.
 26. Pecson BM, Ackermann M, Kohn T. 2011. Framework for using quantitative PCR as a nonculture based method to estimate virus infectivity. *Environ. Sci. Technol.* 45:2257–2263.
 27. Du H, Fuh RCA, Li JZ, Corkan LA, Lindsey JS. 1998. PhotochemCAD: a computer-aided design and research tool in photochemistry. *Photochem. Photobiol.* 68:141–142.
 28. Wigginton KR, Pecson BM, Sigstam T, Bosshard F, Kohn T. 2012. Virus inactivation mechanisms: impact of disinfectants on virus function and structural integrity. *Environ. Sci. Technol.* 46:12069–12078.
 29. Laemmli UK. 1970. Cleavage of structural proteins during the assembly of the head of bacteriophage T4. *Nature* 227:680–685.
 30. Shevchenko A, Wilm M, Vorm O, Mann M. 1996. Mass spectrometric sequencing of proteins from silver stained polyacrylamide gels. *Anal. Chem.* 68:850–858.
 31. Hornstra LM, Smeets P, Medema GJ. 2011. Inactivation of bacteriophage MS2 upon exposure to very low concentrations of chlorine dioxide. *Water Res.* 45:1847–1855.
 32. Phillips JC, Braun R, Wang W, Gumbart J, Tajkhorshid E, Villa E, Chipot C, Skeel RD, Kale L, Schulten K. 2005. Scalable molecular dynamics with NAMD. *J. Comput. Chem.* 26:1781–1802.
 33. Wang JM, Wolf RM, Caldwell JW, Kollman PA, Case DA. 2004. Development and testing of a general amber force field. *J. Comput. Chem.* 25:1157–1174.
 34. Humphrey W, Dalke A, Schulten K. 1996. VMD: visual molecular dynamics. *J. Mol. Graph. Model.* 14:33–38.
 35. Noss CI, Hauchman FS, Olivieri VP. 1986. Chlorine dioxide reactivity with proteins. *Water Res.* 20:351–356.
 36. Miller RL, Plagemann PG. 1974. Effect of ultraviolet light on mengovirus. Formation of uracil dimers, instability and degradation of capsid, and covalent linkage of protein to viral RNA. *J. Virol.* 13:729–739.
 37. Wigginton KR, Menin L, Sigstam T, Gannon G, Cascella M, Ben Hamidane H, Tsybin YO, Waridel P, Kohn T. 2012. UV radiation induces genome-mediated, site-specific cleavage in viral proteins. *Chem-biochem* 13:837–845.
 38. Schneider JE, Tabatabaie T, Maitt L, Smith RH, Nguyen X, Pye Q, Floyd RA. 1998. Potential mechanisms of photodynamic inactivation of virus by methylene blue. I. RNA-protein crosslinks and other oxidative lesions in Q beta bacteriophage. *Photochem. Photobiol.* 67:350–357.
 39. Jensen RL, Arnbjerg J, Ogilby PR. 2012. Reaction of singlet oxygen with tryptophan in proteins: a pronounced effect of the local environment on the reaction rate. *J. Am. Chem. Soc.* 134:9820–9826.
 40. Dennis WH, Olivieri VP, Kruse CW. 1979. Mechanism of disinfection. Incorporation of Cl-36 into f2 virus. *Water Res.* 13:363–369.
 41. Stewart DJ, Napolitano MJ, Bakhmutova-Albert EV, Margerum DW. 2008. Kinetics and mechanisms of chlorine dioxide oxidation of tryptophan. *Inorg. Chem.* 47:1639–1647.
 42. Davies MJ. 2005. The oxidative environment and protein damage. *Biochim. Biophys. Acta* 1703:93–109.